scientific reports

Check for updates

OPEN

Perpendicular magnetic anisotropy, tunneling magnetoresistance and spin-transfer torque effect in magnetic tunnel junctions with Nb layers

Bowei Zhou[1], Pravin Khanal[1], Onri Jay Benally[2], Deyuan Lyu[2], Daniel B. Gopman[3], Arthur Enriquez[1], Ali Habiboglu[1], Kennedy Warrilow[1], Jian-Ping Wang[2] & Wei-Gang Wang[1]✉

Nb and its compounds are widely used in quantum computing due to their high superconducting transition temperatures and high critical fields. Devices that combine superconducting performance and spintronic non-volatility could deliver unique functionality. Here we report the study of magnetic tunnel junctions with Nb as the heavy metal layers. An interfacial perpendicular magnetic anisotropy energy density of 1.85 mJ/m^2 was obtained in Nb/CoFeB/MgO heterostructures. The tunneling magnetoresistance was evaluated in junctions with different thickness combinations and different annealing conditions. An optimized magnetoresistance of 120% was obtained at room temperature, with a damping parameter of 0.011 determined by ferromagnetic resonance. In addition, spin-transfer torque switching has also been successfully observed in these junctions with a quasistatic switching current density of 7.3 × 10^5 A/cm^2.

Magnetic tunnel junctions (MTJs)[1–7] are critical components in magnetic random access memory (MRAM)[8,9], spin-logic[10,11], spin-torque oscillator[12–14], and neuromorphic[15] applications. Particularly, MTJs with perpendicular magnetic easy-axis (pMTJs) are promising due to their potential in ultrafast and ultralow energy operations[16–19], and deep scaling capability down to a lateral size of 2–3 nm[20]. The perpendicular magnetic anisotropy (PMA) in many of these pMTJs has an interfacial origin, where the thickness of the ferromagnetic (FM) layer has to be maintained around 1 nm[21–23]. Typically the MgO barrier is sandwiched by two such thin FM layers, forming the core structure of the pMTJ. The other side of the thin FM layer is usually interfaced with a heavy metal (HM) layer. The perpendicular easy axis of the system is established due to the proper hybridization of the 3*d* wavefunction of the FM layer and the 2*p* wavefunction of the oxygen from the MgO barrier, which can be further influenced by the 3*d*–4*d* or 3*d*–5*d* hybridization at the FM/HM interfaces[21–23]. Clearly in this case the magnetic and transport properties of pMTJs are sensitively dependent on the HM layers. A variety of HM layers such as Pt[24], Ta[16,25], Mo[26–28], and W[22,29] have been explored to investigate the performance of pMTJs.

Niobium (Nb) and its compounds are one of the most important components in quantum computation due to their high superconductivity transition temperatures and high critical fields[30]. In addition to quantum computing, it is also interesting to study the behavior of pMTJs with Nb for cryogenic memory applications. In hybrid magnetic-superconducting devices the two order parameters (magnetism and superconductivity) can influence each other, where novel functionalities can be realized by controlling the two competing orders[31]. In addition, it has been demonstrated recently that the magnetic anisotropy of Fe can be modified by the superconductivity of Vanadium in the MgO/Fe MTJs at low temperatures[32]. On the other hand, electrically modifying the magnetic properties of 3*d* ferromagnets is important in many applications at room temperature (RT)[33–35]. For example, through the voltage-controlled magnetic anisotropy (VCMA) effect[34,36], a switching energy as low as a few femtojoules has been achieved in pMTJs[16–19]. Therefore it would be interesting to investigate the potential interaction between superconductivity and PMA, as well as the VCMA effect in Nb-based pMTJs. In the past,

[1]Department of Physics, University of Arizona, Tucson, AZ 85721, USA. [2]Department of Electrical & Computer Engineering, University of Minnesota, Minneapolis, MN 55455, USA. [3]Materials Science & Engineering Division, National Institute of Standards and Technology, Gaithersburg, MD 20899, USA. ✉email: wgwang@arizona.edu

Nb has been successfully employed to obtain PMA in Nb/CoFeB/MgO heterostructures and the interfacial PMA energy density of 2.2 mJ/m^2 was obtained[37–39]. However, transport properties have not been evaluated in MTJs with Nb layers.

In this study, we report the RT performance of pMTJs with Nb as the HM layers. Magnetic, transport, and spin-dynamic properties of the junctions were investigated in blanket MTJ films as well as patterned junctions. The PMA and the thermal robustness of the pMTJs were studied by varying the thickness of the Nb layers and annealing conditions. A reasonably large TMR of 120% was obtained at RT. Spin-transfer torque (STT)[40,41] switching has also been successfully observed in these junctions with a quasistatic switching current density of 7.3×10^5 A/cm^2.

The MTJ films in this work were fabricated in a 12-source UHV sputtering system (AJA International) with a base pressure of 10^{-7} Pa (10^{-9} Torr). Circular junctions with diameters ranging from 100 nm to 100 μm were patterned and subsequently annealed under varying conditions. Detailed information on sample fabrication and characterization can be found in our previous publications[42–44].

First, the magnetic properties of the films were studied by vibrating sample magnetometry (VSM) as shown in Fig. 1. To isolate the role of the Nb buffer layer on the magnetic properties of CoFeB, a multilayered stack of Si/SiO_2/Ta(3)/Ru(5)/Ta(3)/Nb(10)/$Co_{20}Fe_{60}B_{20}$(0.8–2.2)/MgO(2)/Ta(10)/Ru(20) was fabricated, where numbers in parentheses are thicknesses in nm. Figure 1a shows the easy axis along the out-of-plane direction for the sample with 0.98 nm CoFeB. The saturation magnetization (M_s) and the anisotropy field ($\mu_0 H_k$) of this sample was determined to be 1162 kA/m (1162 emu/cm^3) and 0.67 T, respectively. The easy axis changes to the in-plane direction when the top CoFeB layer is thicker than 1.85 nm and the hysteresis loops of the sample with a 2.08 nm top CoFeB is shown in Fig. 1b. For each sample, the effective perpendicular magnetic anisotropy energy density (E_{eff}) can be obtained as $E_{eff} = \frac{1}{2} M_s \cdot H_k$. The interfacial PMA energy density (E_i) can be obtained by $E_{eff} = E_b - 2\pi M_s^2 + \frac{E_i}{t}$, where E_b and $2\pi M_s^2$ are bulk anisotropy energy density and shape anisotropy energy density, respectively, and t is the thickness of CoFeB on top of MgO. In Fig. 1c, $E_{eff} \cdot t$ is plotted as a function of t, and the y-intercept gives E_i, which is found to be 1.85 mJ/m^2 (1.85 erg/cm^2) in this study for the samples annealed at 300 °C for 10 min. Unfortunately, PMA could not be maintained when the films were annealed at 400 °C. More research is needed as stability at 400 °C is required by the back-end-of-line integration of MTJ with CMOS. It was widely recognized that the formation energy between the HM layer and Fe (60% Fe in the CoFeB alloy used here) plays an important role in determining the thermal stability of pMTJs during annealing[23,27]. Generally, larger formation energy indicates the HM layer and Fe are less likely to diffuse into each other to form compounds. The formation energy of Nb–Fe is about − 23 kJ/mol, which is substantially smaller than that of Mo–Fe (− 3 kJ/mol), but it is similar to Ta–Fe (− 22 kJ/mol)[45]. From this point of view the thermal stability of Nb-pMTJs can be potentially increased to a degree that is similar to Ta-pMTJs through additional materials and process engineering.

Next, the TMR of the Nb-pMTJ was investigated in a series of samples with the structure: Si/SiO_2/Ta(8)/Ru(7)/Ta(9)/Nb(10)/$Co_{20}Fe_{60}B_{20}$(1)/MgO(0.9–3.5)/$Co_{20}Fe_{60}B_{20}$(0.9–1.4)/Nb(10)/Ta(5)/Ru(15), where numbers in parentheses are thicknesses in nm and hyphenated numbers indicate a linearly varying thickness in certain

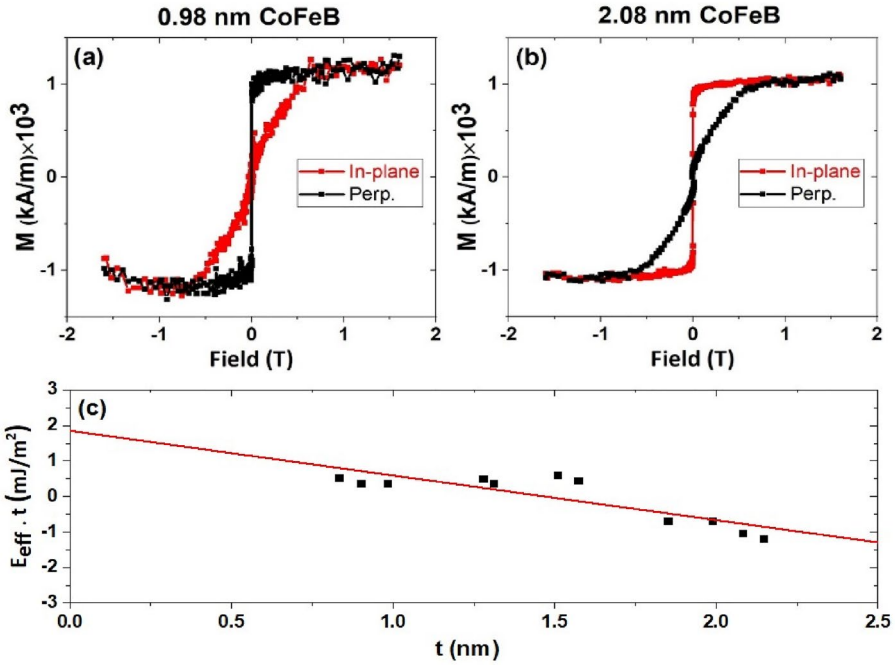

Figure 1. (**a**) and (**b**) Hysteresis loops of the samples with CoFeB thicknesses of 0.98 and 2.08 nm, respectively. The samples were annealed at 300 °C for 10 min. (**c**) The plot of $E_{eff} \cdot t$ as a function of the CoFeB thickness t in a series of samples.

layers across the specimen. Figure 2a shows the thickness dependence of the TMR of these junctions after different annealing. After the 260 °C annealing, the TMR values (blue triangles) almost stayed the same (about 90%) when the thickness of the top CoFeB layer varies from 0.95 to 1.25 nm. After 300 °C annealing for 10 min (green squares), the TMR ratios were reduced in the junctions where the top CoFeB layer is thinner than 1.05 nm, as shown in Fig. 2b. This is likely due to a substantial magnetic dead layer thickness that has a more pronounced impact on the pMTJs with thinner CoFeB. The top CoFeB likely becomes superparamagnetic in this region. However, the maximum TMR increased to 120% with a 1.14 nm thick top CoFeB layer as shown in Fig. 2c, where a broad high-resistance plateau for the AP state and sharp switching for both the top and the bottom CoFeB layers can be seen. It is known that the thermal annealing is critical in determining the magnetoresistance[46] and defects level[47,48] in MTJs, and the increase of TMR is expected through the solid state epitaxy of CoFeB/MgO/CoFeB heterostructures[46,49–51]. But when the top CoFeB is too thick, such as 1.35 nm in this study (as shown in Fig. 2d), it exhibits in-plane anisotropy instead of PMA, which is the reason that there is a linear dependence of resistance for the top layer. The decrease of TMR (to nearly 15%) is more obvious in junctions with thinner top CoFeB after annealing at 350 °C (red dots). Finally, TMRs entirely collapsed after annealing at 400 °C as shown by the black diamonds. The evolution of TMRs for a pMTJ with 1.14 nm of top CoFeB is plotted in Fig. 2c, f, g, after the annealing at 300, 350 and 400 °C, respectively. These figures can be examined with Fig. 2e, where the TMR curve for an MTJ with a very similar thickness of top CoFeB (1.16 nm) annealed at 260 °C is shown. Good PMA for both top and bottom CoFeB layers can be seen after annealing at 260 and 300 °C. The squareness of the perpendicular easy axis in the top CoFeB layer underwent a marked deterioration after annealing at 350 °C, accompanied by a reduced TMR at 94%. Finally, the perpendicular magnetization of both CoFeB layers was lost after the annealing at 400 °C and the TMR further dropped to 8%. These results, namely TMR drops at higher temperatures (and drops faster in devices with thinner CoFeB at a given temperature), are likely caused by the interdiffusion of Nb with CoFeB, consistent with the relatively low Fe-Nb formation energy discussed above.

It was discovered previously that a thin dusting layer of Mo inserted between the Ta and CoFeB layers could give rise to a TMR ratio that is higher than using thick Ta or Mo layers. The TMR enhancement was attributed to the improved thermal stability brought by the Mo dusting layer (< 1 nm), and the unique feature of Ta as an effective Boron sink[23]. Here a series of pMTJs with different Nb layer thicknesses were fabricated: Si/SiO_2/

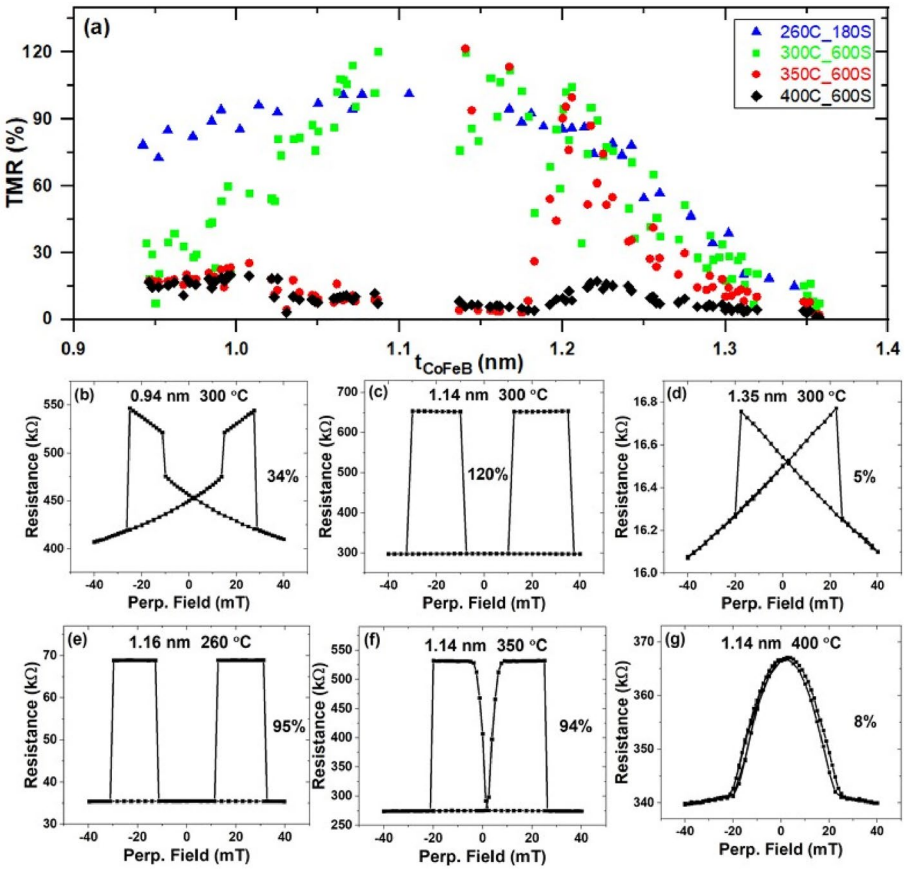

Figure 2. (**a**) Evolution of TMR in Nb-pMTJs with different top CoFeB layer thicknesses after annealing under several different conditions. The samples were successively annealed at 260 °C for 3 min, 300 °C for 10 min, 350 °C for 10 min, and 400 °C for 10 min. (**b**–**d**) TMR hysteresis curves with (**b**) 0.94 nm, (**c**) 1.14 nm, (**d**) 1.35 nm top CoFeB thickness after the 300 °C annealing for 10 min. (**e**–**g**) TMR curves under different annealing conditions with similar top CoFeB thicknesses (around 1.14 nm).

Ta(8)/Ru(7)/Ta(9)/Nb (d_1)/$Co_{20}Fe_{60}B_{20}$(1)/MgO(0.9–3.5)/ $Co_{20}Fe_{60}B_{20}$(0.9–1.4)/Nb(d_2)/Ta(5)/Ru(15), where d_1 and d_2 represent different Nb thicknesses. The TMR measurement was investigated after annealing at 300 °C for 10 min. Relatively small TMR ratios, 91%, and 93% were found in the junctions with 0.7 and 3 nm of buffer Nb as shown in Fig. 3a and b, respectively. The low TMR is related to the lack of a good AP plateau, due to the weak PMA of the top CoFeB layers. The TMR ratios of these junctions are smaller than that of the 120% observed in the pMTJ with 10 nm of buffer Nb as shown in Fig. 2c. However, further increasing the thickness of Nb beyond 10 nm turned out to be deleterious—the TMR ratio is reduced to 80% with 20 nm buffer Nb as shown in Fig. 3c. Previously a superconducting critical temperature of about 6 K was measured in an 8 nm-thick Nb film[52]. Therefore Nb films with the thickness of 10 nm and 20 nm in our structures are likely to be superconducting as well at low temperatures.

The spin dynamics of the samples were evaluated by broadband ferromagnetic resonance (FMR) measurements in Nb-pMTJs with $d_1 = 20$ nm and $d_2 = 10$ nm. To increase the FMR sensitivity, an eternal field H_{ext} was modulated ($\mu_0 H_{mod} = 1$ mT peak amplitude) and a lock-in detection scheme was used, whereby FMR spectra were measured at fixed microwave frequencies (20–40 GHz) under a swept H_{ext}. Figure 3d shows illustrative FMR measurements for perpendicular H_{ext}, from which we extract the frequency-dependent resonance field H_{res}, and the linewidth ΔH. The solid lines reflect the best fit of the raw absorption data. The ferromagnetic resonance relationship between microwave excitation frequency and resonant perpendicular applied magnetic field is given by: $\left(\frac{f}{\gamma}\right)^{\perp} = \mu_0 H_{res} + \mu_0 H_{eff}^{\perp}$, and linewidth versus frequency dispersion are given by: $\mu_0 \Delta H = \frac{2\alpha}{\gamma} f + \mu_0 \Delta H_0$, where $f^{\perp}$ is the FMR frequency, γ is the gyromagnetic ratio, μ_0 is the vacuum permeability, α is the Gilbert damping parameter and $\mu_0 H_{eff}^{\perp} = \mu_0 H_K - \mu_0 M_s$ is the effective perpendicular anisotropy field. FMR signals from both the top and bottom CoFeB layers of the pMTJ are shown in Fig. 3d. The effective anisotropy field was determined to be 0.58 T for the sample annealed at 260 °C for 3 min. From the fitting of f versus frequency $\mu_0 H_{res}$ (Fig. 3e) and the fitting of $\mu_0 \Delta H$ versus frequency f (Fig. 3f), the Gilbert damping factor α for the bottom CoFeB layer is extracted to be 0.011 for the sample annealed at 260 °C, which increased slightly to 0.013 after the annealing at 300 °C. These α values are similar to those found in W/CoFeB/MgO and Ta/CoFeB/MgO structures[53].

Finally, we investigated the STT effect in the pMTJs with Nb as the capping layer. The core structure of these pMTJs for studying STT is Si/SiO_2/Ta(8)/Ru(7)/Ta(9)/Mo(1.2)/$Co_{20}Fe_{60}B_{20}$(1)/MgO(0.9)/$Co_{20}Fe_{60}B_{20}$(1.2–1.7)/Nb(10)/Ta(5)/Ru(7), where numbers in parentheses are thicknesses in nm. Since the free layer is the CoFeB above the MgO, $d_1 = 0$, and $d_2 = 10$ nm were employed in these junctions to study the impact of Nb adjacent to the free layer. The magnetoresistance curve of a 145 nm device is plotted as black squares in Fig. 4a, where the TMR ratio is 101% with a resistance area product of 107 Ω·μm^2. The current-induced switching of resistance is plotted by the red dots in the same figure. The pMTJ can be fully switched between the *P* and *AP* states by the

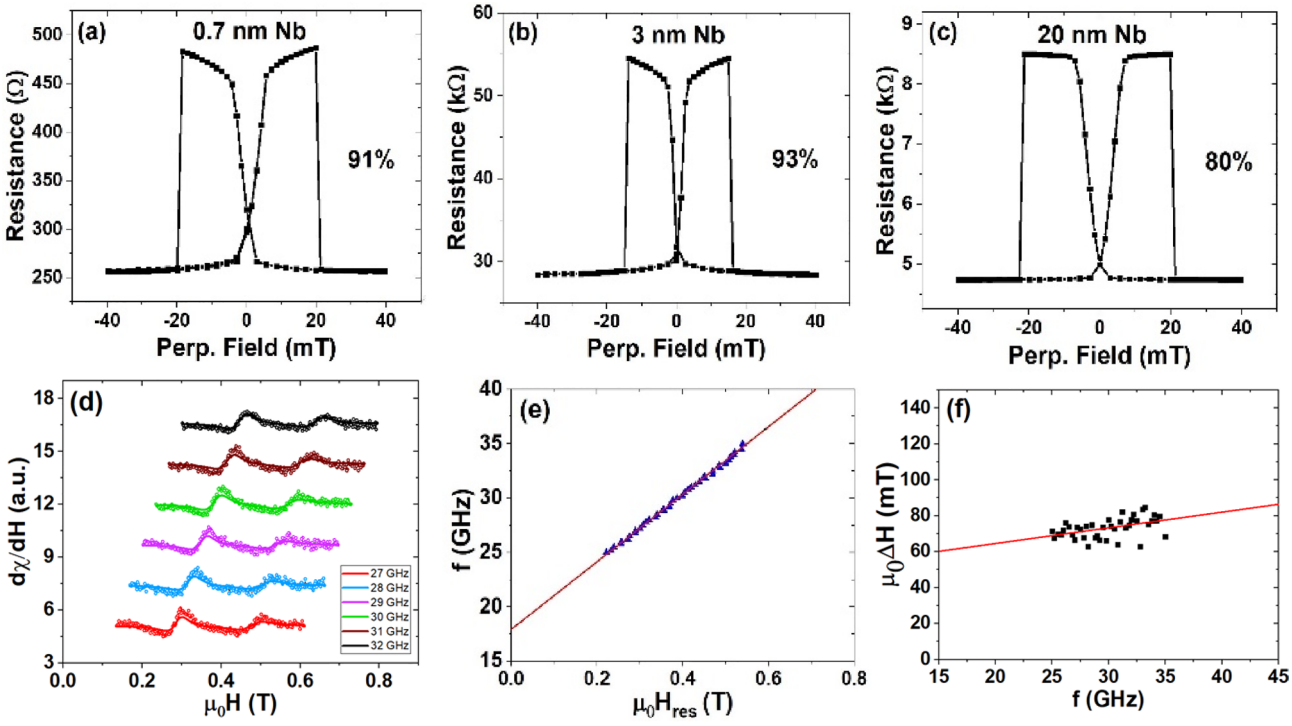

Figure 3. The TMRs of a series of pMTJs with (**a**) $d_1 = 0.7$ nm, $d_2 = 1.18$ nm; (**b**) $d_1 = 3$ nm, $d_2 = 3$ nm; (**c**) $d_1 = 20$ nm, $d_2 = 10$ nm; after being annealed at 300 °C for 10 min. (**d**) Ferromagnetic resonance (FMR) measurements in Nb-pMTJs with FMR frequencies between 27 and 32 GHz. (**e**) The fitting of the FMR frequency f versus frequency-dependent resonance field $\mu_0 H_{res}$. (**f**) The fitting of the linewidth $\mu_0 \Delta H$ versus the FMR frequency f.

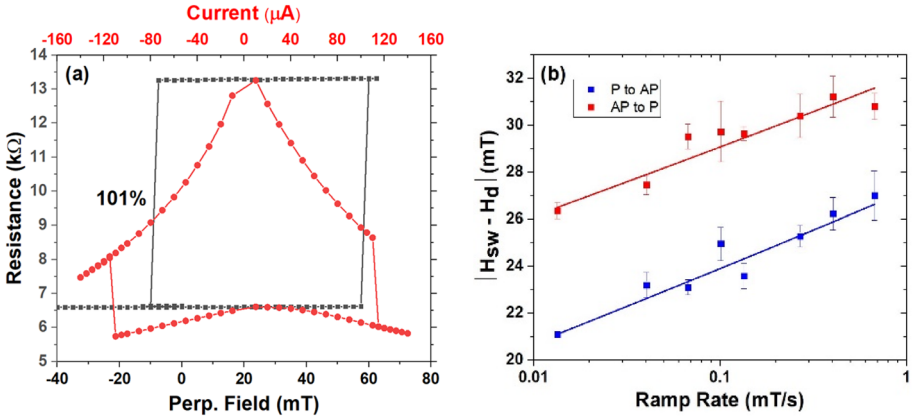

Figure 4. (**a**) The TMR curve of the 145 nm-diameter MTJ nanopillar with 101% TMR ratio (black squares) and the current-induced resistance switching (red dots) by the STT effect. (**b**) The ramp-rate-dependent switching field measurements for both P-to-AP and AP-to-P transitions.

STT effect and the switching current is around 120 μA, corresponding to a quasistatic switching current density of 7.3×10^5 A/cm^2. An external field of 24 mT was applied to offset the dipolar field during the current-induced switching experiment. To determine the thermal stability of the pMTJ, we measured the TMR curves under different ramp rates of the magnetic field. The switching field should take the form[54]

$$< H_c >=< H_{sw} - H_d >= H_{c0}(T)\left\{1 - \left[\frac{k_B T}{E_a}\ln\left(\frac{1}{\tau_0 |R_H| \ln 2}\right)\right]^{\frac{2}{3}}\right\}, \quad (1)$$

where k_B is Boltzmann's constant, R_H is the ramp rate for the field, H_{sw} is the switching field, and H_d is the dipole field from the reference layer. From the fits to the field-ramp data in Fig. 4b, we obtain $E_{P\text{-}AP} = 1$ eV (corresponding to the thermal stability factor $\Delta = 40$) for P-to-AP switching, and $E_{AP\text{-}P} = 1.18$ eV (corresponding to $\Delta = 47$) for AP-to-P switching.

In summary, we have investigated the magnetic, transport, and spin dynamic properties of the MTJs with Nb as the HM layers. Our results here demonstrate the compatibility of Nb with high-quality pMTJs, as reflected by the sizable TMR, the reasonably small damping parameter, and STT switching current density. These findings may be useful for future quantum computing and cryogenic memory applications, as well as the exploration of various new phenomena related to the interaction of spin and superconductivity.

Data availability

The data that support the findings of this study are available from the corresponding author upon reasonable request.

Received: 5 December 2022; Accepted: 9 February 2023
Published online: 01 March 2023

References

1. Moodera, J. S., Kinder, L. R., Wong, T. M. & Meservey, R. Large magnetoresistance at room-temperature in ferromagnetic thin-film tunnel-junctions. *Phys. Rev. Lett.* **74**, 3273–3276 (1995).
2. Miyazaki, T. & Tezuka, N. Giant magnetic tunneling effect in Fe/Al_2O_3/Fe junction. *J. Magn. Magn. Mater.* **139**, 94–97 (1995).
3. Parkin, S. S. P. *et al.* Giant tunnelling magnetoresistance at room temperature with MgO (100) tunnel barriers. *Nat. Mater.* **3**, 862–867 (2004).
4. Yuasa, S., Nagahama, T., Fukushima, A., Suzuki, Y. & Ando, K. Giant room-temperature magnetoresistance in single-crystal Fe/MgO/Fe magnetic tunnel junctions. *Nat. Mater.* **3**, 868–871 (2004).
5. Butler, W. H., Zhang, X.-G., Schulthess, T. C. & MacLaren, J. M. Spin-dependent tunneling conductance of Fe|MgO|Fe sandwiches. *Phys. Rev. B* **63**, 054416 (2001).
6. Zhu, J. & Park, C. Magnetic tunnel junctions. *Mater. Today* **9**, 36–45 (2006).
7. Tsymbal, E. Y., Mryasov, O. N. & LeClair, P. R. Spin-dependent tunnelling in magnetic tunnel junctions. *J. Phys. Condens. Matter* **15**, R109–R142 (2003).
8. Tehrani, S. *et al.* Magnetoresistive random access memory using magnetic tunnel junctions. *Proc. IEEE* **91**, 703–714 (2003).
9. Kent, A. D. & Worledge, D. C. A new spin on magnetic memories. *Nat. Nanotechnol.* **10**, 187 (2015).
10. Behtash Behin-Aein, D. D., Salahuddin, S. & Datta, S. Proposal for an all-spin logic device with built-in memory. *Nat. Nanotechnol.* **5**, 266 (2010).
11. Wang, J., Meng, H. & Wang, J. P. Programmable spintronics logic device based on a magnetic tunnel junction element. *J. Appl. Phys.* **97**, 10D509 (2005).
12. Kaka, S. *et al.* Mutual phase-locking of microwave spin torque nano-oscillators. *Nature* **437**, 389–392 (2005).
13. Krivorotov, I. N. *et al.* Time-domain measurements of nanomagnet dynamics driven by spin-transfer torques. *Science* **307**, 228–231 (2005).

14. Liu, R., Lim, W. & Urazhdin, S. Spectral characteristics of the microwave emission by the spin hall nano-oscillator. *Phys. Rev. Lett.* **110**, 147601 (2013).
15. Sengupta, A., Han, B. & Roy, K. Toward a spintronic deep learning spiking neural processor. In *2016 IEEE Biomedical Circuits and Systems Conference* 544–547 (IEEE, 2016). https://doi.org/10.1109/BioCAS.2016.7833852.
16. Ikeda, S. *et al.* A perpendicular-anisotropy CoFeB–MgO magnetic tunnel junction. *Nat. Mater.* **9**, 721–724 (2010).
17. Grezes, C. *et al.* Ultra-low switching energy and scaling in electric-field-controlled nanoscale magnetic tunnel junctions with high resistance-area product. *Appl. Phys. Lett.* **20**, 2–5 (2016).
18. Kanai, S., Matsukura, F. & Ohno, H. Electric-field-induced magnetization switching in CoFeB/MgO magnetic tunnel junctions with high junction resistance. *Appl. Phys. Lett.* **108**, 192406 (2016).
19. Yamamoto, T. *et al.* Write-error reduction of voltage-torque-driven magnetization switching by a controlled voltage pulse. *Phys. Rev. Appl.* **11**, 014013 (2019).
20. Jinnai, B., Igarashi, J., Watanabe, K., Funatsu, T., Sato, H., Fukami, S. & Ohno, H. High-performance shape-anisotropy magnetic tunnel junctions down to 2.3 nm. In *2020 IEEE International Electron Devices Meeting (IEDM)* (2020).
21. Dieny, B. & Chshiev, M. Perpendicular magnetic anisotropy at transition metal/oxide interfaces and applications. *Rev. Mod. Phys.* **89**, 025008 (2017).
22. Almasi, H. *et al.* Perpendicular magnetic tunnel junction with W seed and capping layers. *J. Appl. Phys.* **121**, 153902 (2017).
23. Almasi, H., Xu, M., Xu, Y., Newhouse-Illige, T. & Wang, W. G. Effect of Mo insertion layers on the magnetoresistance and perpendicular magnetic anisotropy in Ta/CoFeB/MgO junctions. *Appl. Phys. Lett.* **109**, 032401 (2016).
24. Lee, D. Y., Shim, T. H. & Park, J. G. Effects of Pt capping layer on perpendicular magnet anisotropy in pseudo-spin valves of Ta/CoFeB/MgO/CoFeB/Pt magnetic-tunneling junctions. *Appl. Phys. Lett.* **102**, 212409 (2013).
25. Worledge, D. C. *et al.* Spin torque switching of perpendicular Ta|CoFeB|MgO-based magnetic tunnel junctions. *Appl. Phys. Lett.* **98**, 022501 (2011).
26. Liu, T., Zhang, Y., Cai, J. W. & Pan, H. Y. Thermally robust Mo/CoFeB/MgO trilayers with strong perpendicular magnetic anisotropy. *Sci. Rep.* **4**, 5895 (2014).
27. Almasi, H. *et al.* Enhanced tunneling magnetoresistance and perpendicular magnetic anisotropy in Mo/CoFeB/MgO magnetic tunnel junctions. *Appl. Phys. Lett.* **106**, 182406 (2015).
28. Cheng, H. *et al.* Giant perpendicular magnetic anisotropy in Mo-based double-interface free layer structure for advanced magnetic tunnel junctions. *Adv. Electron. Mater.* **6**, 1–8 (2020).
29. Chatterjee, J. *et al.* Enhanced annealing stability and perpendicular magnetic anisotropy in perpendicular magnetic tunnel junctions using W layer. *Appl. Phys. Lett.* **110**, 202401 (2017).
30. Murray, C. E. Material matters in superconducting qubits. *Mater. Sci. Eng. R Rep.* **146**, 100646 (2021).
31. Baek, B., Rippard, W. H., Benz, S. P., Russek, S. E. & Dresselhaus, P. D. Hybrid superconducting-magnetic memory device using competing order parameters. *Nat. Commun.* **5**, 1–6 (2014).
32. González-Ruano, C. *et al.* Superconductivity assisted change of the perpendicular magnetic anisotropy in V/MgO/Fe junctions. *Sci. Rep.* **11**, 1–10 (2021).
33. Bi, C. *et al.* Reversible control of Co magnetism by voltage-induced oxidation. *Phys. Rev. Lett.* **113**, 267202 (2014).
34. Matsukura, F., Tokura, Y. & Ohno, H. Control of magnetism by electric fields. *Nat. Nanotechnol.* **10**, 209–220 (2015).
35. Bi, C. *et al.* Electrical control of metallic heavy-metal-ferromagnet interfacial states. *Phys. Rev. Appl.* **8**, 034003 (2017).
36. Wang, W.-G., Li, M., Hageman, S. & Chien, C. L. Electric-field-assisted switching in magnetic tunnel junctions. *Nat. Mater.* **11**, 64–68 (2012).
37. Cheng, T. I., Cheng, C. W. & Chern, G. Perpendicular magnetic anisotropy induced by a cap layer in ultrathin MgO/CoFeB/Nb. *J. Appl. Phys.* **112**, 3–7 (2012).
38. Li, M., Wang, S., Zhang, S., Fang, S. & Yu, G. The perpendicular magnetic anisotropies of CoFeB/MgO films with Nb buffer layers. *J. Magn. Magn. Mater.* **485**, 187–192 (2019).
39. Lee, D. S., Chang, H. T., Cheng, C. W. & Chern, G. Perpendicular magnetic anisotropy in MgO/CoFeB/Nb and a comparison of the cap layer effect. *IEEE Trans. Magn.* **50**, 1–4 (2014).
40. Ralph, D. C. & Stiles, M. D. Spin transfer torques. *J. Magn. Magn. Mater.* **320**, 1190–1216 (2008).
41. Brataas, A., Kent, A. D. & Ohno, H. Current-induced torques in magnetic materials. *Nat. Mater.* **11**, 372–381 (2012).
42. Xu, M. *et al.* Voltage-controlled antiferromagnetism in magnetic tunnel junctions. *Phys. Rev. Lett.* **124**, 187701 (2020).
43. Khanal, P. *et al.* Perpendicular magnetic tunnel junctions with multi-interface free layer Perpendicular magnetic tunnel junctions with multi-interface free layer. *Appl. Phys. Lett.* **119**, 242404 (2021).
44. Wang, W. G. *et al.* Parallel fabrication of magnetic tunnel junction nanopillars by nanosphere lithography. *Sci. Rep.* **3**, 1948 (2013).
45. Boer, F. R. D. *Cohesion in Metals* (North-Holland, 1988).
46. Wang, W. G. *et al.* Understanding tunneling magnetoresistance during thermal annealing in MgO-based junctions with CoFeB electrodes. *Phys. Rev. B* **81**, 144406 (2010).
47. Wang, W. G. *et al.* Spin-polarized transport in hybrid (Zn, Cr)Te/Al_2O_3/Co magnetic tunnel junctions. *Appl. Phys. Lett.* **88**, 202501 (2006).
48. Stearrett, R., Wang, W. G., Shah, L. R., Xiao, J. Q. & Nowak, E. R. Magnetic noise evolution in CoFeB/MgO/CoFeB tunnel junctions during annealing. *Appl. Phys. Lett.* **97**, 243502 (2010).
49. Choi, Y. S., Tsunekawa, K., Nagamine, Y. & Djayaprawira, D. Transmission electron microscopy study on the polycrystalline CoFeB/MgO/CoFeB based magnetic tunnel junction showing a high tunneling magnetoresistance, predicted in single crystal magnetic tunnel junction. *J. Appl. Phys.* **101**, 013907 (2007).
50. Wang, W. G. *et al.* Real-time evolution of tunneling magnetoresistance during annealing in CoFeB/MgO/CoFeB magnetic tunnel junctions. *Appl. Phys. Lett.* **92**, 152501 (2008).
51. Wang, W. G. *et al.* In situ characterization of rapid crystallization of amorphous CoFeB electrodes in CoFeB/MgO/CoFeB junctions during thermal annealing. *Appl. Phys. Lett.* **95**, 242501 (2009).
52. Gubin, A. I., Ilin, K. S., Vitusevich, S. A., Siegel, M. & Klein, N. Dependence of magnetic penetration depth on the thickness of superconducting Nb thin films. *Phys. Rev. B Condens. Matter Mater. Phys.* **72**, 064503 (2005).
53. Lattery, D. M. *et al.* Low Gilbert damping constant in perpendicularly magnetized W/CoFeB/MgO films with high thermal stability. *Sci. Rep.* **8**, 1–9 (2018).
54. Sharrock, M. P. Time-dependent magnetic phenomena and particle-size effects in recording media. *IEEE Trans. Magn.* **26**, 193–197 (1990).

Acknowledgements

This work was supported in part by Semiconductor Research Corporation through the Logic and Memory Devices program, by DARPA through the ERI program (FRANC), and by NSF through DMR-1905783. A.E. and K.W. were supported by the REU supplement of NSF ECCS-1554011.

Author contributions

P.K. made the multilayers of the sample; O.J.B. and D.L. did the ion beam etching; D.B.G. did the Ferromagnetic Resonance (FMR) measurements; B.Z., A.E., A.H., K.W. did the TMR measurements; B.Z. also did the STT and thermal stability factor measurements, and prepared all the figures. B.Z. and W.W. wrote the manuscript; J.-P.W. and W.-G.W. provided guidance for the project; and all authors reviewed the manuscript.

Competing interests

The authors declare no competing interests.

Additional information

Correspondence and requests for materials should be addressed to W.-G.W.

Reprints and permissions information is available at www.nature.com/reprints.

Publisher's note Springer Nature remains neutral with regard to jurisdictional claims in published maps and institutional affiliations.